

# The Kohn–Luttinger Mechanism and Phase Diagram of the Superconducting State in the Shubin–Vonsovsky Model

M. Yu. Kagan<sup>a,\*</sup>, V. V. Val'kov<sup>b,c</sup>, V. A. Mitskan<sup>b,c</sup>, and M. M. Korovuskin<sup>b,c</sup>

<sup>a</sup>Kapitza Institute for Physical Problems, Russian Academy of Sciences, Moscow, 119334 Russia

<sup>b</sup>Kirenskii Physics Institute, Siberian Branch, Russian Academy of Sciences, Krasnoyarsk, 660036 Russia

<sup>c</sup>Reshetnev Siberian Aerospace University, Krasnoyarsk, 660014 Russia

\*e-mail: kagan@kapitza.ras.ru

Received March 27, 2013

**Abstract**—Using the Shubin–Vonsovsky model in the weak-coupling regime  $W > U > V$  ( $W$  is the bandwidth,  $U$  is the Hubbard onsite repulsion, and  $V$  is the Coulomb interaction at neighboring sites) based on the Kohn–Luttinger mechanism, we determined the regions of the existence of the superconducting phases with the  $d_{xy}$ ,  $p$ ,  $s$ , and  $d_{x^2-y^2}$  symmetry types of the order parameter. It is shown that the effective interaction in the Cooper channel considerably depends not only on single-site but also on intersite Coulomb correlations. This is demonstrated by the example of the qualitative change and complication of the phase diagram of the superconducting state. The superconducting (SC) phase induction mechanism is determined taking into account polarization contributions in the second-order perturbation theory in the Coulomb interaction. The results obtained for the angular dependence of the superconducting gap in different channels are compared with angle-resolved photoemission spectroscopy (ARPES) results. The influence of long-range hops in the phase diagram and critical superconducting transition temperature in different channels is analyzed. The conditions for the appearance of the Kohn–Luttinger superconductivity with the  $d_{x^2-y^2}$  symmetry and high critical temperatures  $T_c \sim 100$  K near the half-filling are determined.

DOI: 10.1134/S1063776113120030

## 1. INTRODUCTION

Extensive studies of superfluidity in  $^3\text{He}$  and ultracold quantum Fermi gases and superconductivity in cuprates, heavy-Fermion intermetallic compounds, semimetals and superlattices have stimulated interest in nonconventional mechanisms of the Cooper pairing. One of the most popular nonphonon mechanisms of superconductivity is the Kohn–Luttinger mechanism [1], proposed in 1965. It was shown in [1] that, due to the presence of the long-range component in the effective potential of interaction of particles via the fermionic background, any three-dimensional electron system with the bare repulsive interaction between particles is certainly unstable with respect to the transition to the superconducting state with a large orbital moment of the relative motion of a Cooper pair ( $l \gg 1$ ).

The Kohn–Luttinger mechanism is closely related to Friedel oscillations [2]. It is well known that due to the sharp boundary  $2k_F$  in the electron density distribution in the momentum space at the Fermi level, the impurity potentials in a metal do not decrease monotonically but oscillate (Friedel oscillations [3]). Kohn and Luttinger showed [1] that such oscillations appear in the effective electron–electron interaction, resulting in attraction between two electrons upon averaging over a potential relief of Friedel maxima and minima.

This attraction can in turn cause the Cooper instability in a channel with  $l \neq 0$ .

However, the estimates [1] of the critical temperature for realistic parameters of electron systems in a metal gave very low values for this temperature ( $T_c \sim 10^{-16}$  K for  $^3\text{He}$  and  $T_c \sim 10^{-11}$  K for a metal plasma for  $l = 2$ ). Such a low value of  $T_c$  was one of the reasons why the Kohn–Luttinger mechanism has not interested researchers for a long time.

The asymptotic results of Kohn and Luttinger obtained for large orbital moments  $l \gg 1$  were generalized in [4–6] for the case of arbitrary  $l$ , and it was also shown that a low-density Fermi gas with repulsion is unstable with respect to superconducting  $p$ -wave pairing ( $l = 1$ ) [4–6]. The generalization of the approach used in [4, 5] to the case of superfluid  $^3\text{He}$  [7–11] and an electron plasma in metals [5, 12] gave estimates  $T_c \sim 1$  mK in  $^3\text{He}$  [5, 13] and  $T_c \sim 10$  mK in very clean metals [12].

In addition, a number of important results, such as cascade superconducting transitions with different values of  $l$  in a three-dimensional dense Coulomb plasma [12], were obtained in [12, 14, 15]. Superconductivity in the three-dimensional and two-dimensional Hubbard models with a low electron density was also predicted in [16, 17], and the anomalous superconductivity in heavy-Fermion systems was consid-

ered in [18]. Finally, it was shown in [19, 20] that the critical temperature of superconducting  $p$ -wave pairing in two-dimensional or layered systems can be drastically increased already at low carrier densities by considering the two-band or spin-polarized situation. In this case, a superconducting transition in heterostructures and layered materials [14, 19, 20] (organic superconductors, semimetals, and superlattices) can be expected in the temperature range  $T_c = 1–5$  K.

After the appearance of these papers and the discovery of HTSC systems, the Kohn–Luttinger mechanism attracted considerable attention as a promising mechanism for nonphonon superconductivity in cuprate oxides. Because the experimental data suggested that the superconducting order parameter in these compounds corresponds to the  $d_{x^2-y^2}$  symmetry type, the competition between different symmetry types of the order parameter was actively investigated using this mechanism in the phase diagram of the Hubbard model [21] close to half-filling [22–26]. At present the popularity of the Kohn–Luttinger mechanism is increasing due to the possibility of its implementation in other actual physical systems. For example, the question of the conditions for its realization in doped graphene was recently discussed in [27, 28] and in [29] where topological superfluid liquids were studied [29].

The role of the combined influence of the onsite,  $U$ , and intersite,  $V$ , Coulomb interaction on superconductivity in cuprates within the framework of the Kohn–Luttinger mechanism was recently discussed in [30]. The increasing interest in the problem of accounting for the long-range intersite Coulomb correlations in the description of the phase diagram of the weakly doped Mott–Hubbard systems [31] made the extended Hubbard model, which includes the interaction of electrons located at different crystal lattice sites (this model is often called the Shubnikov–Vonsovsky model in the Russian literature [32, 33]), very popular. This model has been widely used for studying polar states in solids [34], the metal–dielectric transition [35], and the influence of intersite Coulomb interaction on the superconducting properties of strongly correlated electron systems [36–38].

Based on this model and the Kohn–Luttinger mechanism, the authors of [39] constructed the phase diagram, which clearly reflects the result of the competition between superconducting phases with different symmetry types of the order parameter. The effective coupling constant was calculated taking into account only the contributions of the order of  $U^2$  in analytic expressions for Kohn–Luttinger diagrams, while the energy spectrum of electrons was determined in the nearest neighbor approximation. These restrictions significantly simplified the phase diagram of the superconducting state.

As mentioned above, the Kohn–Luttinger mechanism of SC instability is related to Friedel oscillations induced by second-order processes with respect to the

bare interaction. In this case, the possibility of achieving the superconducting state is determined by the matrix elements of the expansion of the effective interaction between electrons in a Cooper channel with the basis functions of the irreducible representations of a two-dimensional square lattice. Therefore, taking into account the terms of the order of  $V^2$  (which have a more complicated momentum dependence) could initiate the contributions of the representations that would make a comparatively small contribution or would be not present at all without an account for this effect. This makes it important to study the conditions for the appearance of the Kohn–Luttinger instability taking into account second-order terms in the intersite Coulomb interaction. Since interference effects caused by the spatial separation of the interacting electrons affect both the effective coupling constant for the specific symmetry type of the order parameter and the coefficients determining the set of the basis functions of the irreducible representation, it is important to take into account the interaction between electrons separated by the distances corresponding not only to the first but also the second coordination sphere. Meanwhile, it is also important to go beyond the nearest-neighbor approximation when simulating the energy spectrum of electrons. This is explained by the fact that the main contribution to the effective coupling constant is determined by the electrons located near the Fermi surface, whose geometry depends on the structure of the energy spectrum. This structure in the Wannier representation is determined both by the number of hopping integrals taken into account and their relative intensity. Therefore, the inclusion of long-range hoppings can modify the phase diagram determining the regions of the realization of the superconducting states with different symmetry types of the order parameter.

In this paper, we consider the effects mentioned above. The Cooper instability in the Shubin–Vonsovsky model is studied in the weak coupling Born approximation  $W > U > V$  ( $W$  is the bandwidth) taking into account the long-range hoppings and the Coulomb interaction of electrons from the first and second coordination spheres. Correspondingly, the scattering amplitude in the Cooper channel is calculated by using the effective interaction  $\tilde{\Gamma}(p, k)$  between two electrons with opposite values of quasi-momentum and spin, which is determined in graphic form by summing up five diagrams in Fig. 1. The first diagram in Fig. 1 corresponds to the bare interaction of two electrons in the Cooper channel and is analytically determined by the expression  $U + V_{\mathbf{p}-\mathbf{k}}$ . The following four diagrams (Kohn–Luttinger diagrams) are related to the second-order scattering processes and take into account polarization effects of the occupied Fermi sphere. One can see that the second-order effective interaction of two electrons in the Cooper channel is determined by processes also involving electrons with the same spin projections. The intensity of such pro-

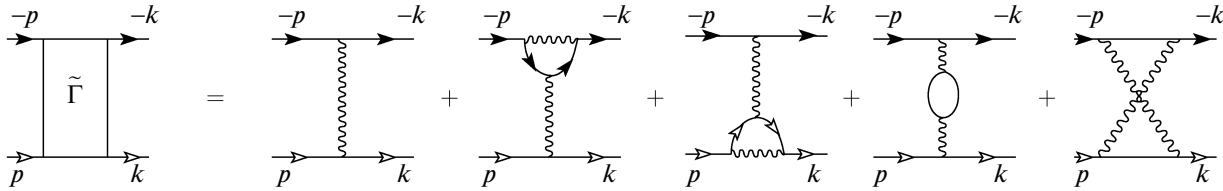


**Fig. 1.** First- and second-order diagrams for effective interaction. Solid straight lines with a light (dark) arrow correspond to the Green's function of electrons with spin projection  $1/2$  ( $-1/2$ ). Wavy lines correspond to the bare interaction.

cesses depends only on the intersite Coulomb interaction.

We have shown in this paper that an account of the long-range Coulomb correlations and long-range electron hoppings significantly affects the conditions for attaining Cooper pairing with the  $s$ -,  $p$ -, and  $d$ -wave symmetry types of order parameter, providing, in particular, the possibility of  $d_{x^2-y^2}$ -wave pairing in rather broad density intervals.

The paper is organized as follows. In Section 2, we discuss the physics of the Shubin–Vonsovsky model and the main approximations used for studying the Kohn–Luttinger superconductivity mechanism. In Section 3, taking into account the contributions from the Kohn–Luttinger diagrams up to and including the second order of perturbation theory inclusive, we obtain the expression for the effective interactions of electrons in the Cooper channel. In Section 4, we briefly describe the method for solving the integral Bethe–Salpeter equation on a two-dimensional square lattice, which includes the renormalized effective interaction. In Section 5, we present the details of the numerical analysis of the system under study. In Section 6, we present the results of the numerical calculations for the superconducting phase diagram in the Shubin–Vonsovsky model, which were obtained both by taking into account long-range Coulomb interactions in second-order perturbation theory and considering long-range electron hoppings. The angular dependence of the order parameter for the  $s$ -wave pairing was compared with recent ARPES experiments in one of the iron-containing superconductors,  $\text{KFe}_2\text{As}_2$ . The results are discussed in the final section.

## 2. SHUBIN–VONSOVSKY MODEL

The Hamiltonian of the Shubin–Vonsovsky model for a square lattice in the single-band approximation can be written in the form

$$\begin{aligned} \hat{H} = & \sum_{f\sigma} (\varepsilon - \mu) c_{f\sigma}^\dagger c_{f\sigma} + \sum_{fm\sigma} t_{fm} c_{f\sigma}^\dagger c_{m\sigma} \\ & + U \sum_f \hat{n}_{f\uparrow} \hat{n}_{f\downarrow} + \frac{V_1}{2} \sum_{f\delta_1} \hat{n}_f \hat{n}_{f+\delta_1} \\ & + \frac{V_2}{2} \sum_{f\delta_2} \hat{n}_f \hat{n}_{f+\delta_2}, \end{aligned} \quad (1)$$

$$+ \frac{V_2}{2} \sum_{f\delta_2} \hat{n}_f \hat{n}_{f+\delta_2},$$

where the first two terms describe an ensemble of non-interacting electrons in the Wannier representation;  $c_{f\sigma}^\dagger$  ( $c_{f\sigma}$ ) is the electron creation (annihilation) operator at site  $f$  with spin projection  $\sigma = \pm 1/2$ ;  $\varepsilon$  is the single-site electron energy;  $\mu$  is the chemical potential of the system; and  $t_{fm}$  is the matrix element (hopping integral) corresponding to the process intensity when an electron is annihilated at site  $m$  and is created at site  $f$ . The third term describes the onsite repulsion of the electrons;  $\hat{n}_{f\sigma} = c_{f\sigma}^\dagger c_{f\sigma}$  is the operator of the electron density at site  $f$  with spin projection  $\sigma$ , and  $\hat{n}_f = \hat{n}_{f\uparrow} + \hat{n}_{f\downarrow}$  is the operator of the total electron density at site  $f$ . The fourth term in (1) takes into account an energy  $V_1$  of the Coulomb interaction of electrons at neighboring sites  $f$  and  $f + \delta_1$ . Finally, the last term in the Hamiltonian (1) takes into account the interaction of electrons at next-to-neighboring sites. The energy of this interaction is specified by the parameter  $V_2$ .

The last three terms of Hamiltonian (1) reflect in combination the fact that the screening radius in the systems under consideration is equal to a few unit cell parameters [35]. The intersite Coulomb interaction in the Shubin–Vonsovsky model is taken into account within a small number of coordination spheres. The bare interaction  $U_{\text{vac}}$  in this model is qualitatively shown in Fig. 2. It is important that the Fourier transform of the bare potential is  $U_{\text{vac}}(\mathbf{q}) = U + V_{\mathbf{q}}$ , where

$$V_{\mathbf{q}} = 2V_1(\cos q_x d + \cos q_y d) + 4V_2 \cos q_x d \cos q_y d,$$

$\mathbf{q}$  is the transferred momentum, and  $d$  is the intersite distance. Note that the potential  $U_{\text{vac}}(\mathbf{q})$  quadratically depends on the quasi-momentum only in the region  $\mathbf{q} \cdot \mathbf{d} \ll 1$ . It is important that the momentum dependence of  $V_{\mathbf{q}}$  beyond this region is determined by the periodic functions. As a result, the behavior of the potential  $U_{\text{vac}}(\mathbf{q})$  is considerably modified compared to the momentum dependence of the Yukawa potential. These factors considerably affect the conditions for the realization of the Cooper instability at high electron densities, when the Fermi surface has no spherical symmetry. Therefore, it can be expected that the conditions for the realization of the superconducting pairing in the framework of the

Kohn–Luttinger mechanism will be determined not only by the dynamic effects caused by Coulomb interactions but also by the influence of the Brillouin zone.

After the Fourier transformation, we obtain

$$\hat{H} = \sum_{\mathbf{p}\sigma} (\varepsilon_{\mathbf{p}} - \mu) c_{\mathbf{p}\sigma}^{\dagger} c_{\mathbf{p}\sigma} + U \sum_{\mathbf{p}\mathbf{p}'\mathbf{q}} c_{\mathbf{p}\uparrow}^{\dagger} c_{\mathbf{p}'+\mathbf{q}\downarrow} c_{\mathbf{p}+\mathbf{q}\downarrow} c_{\mathbf{p}'\uparrow} + \frac{1}{2} \sum_{\mathbf{p}\mathbf{p}'\mathbf{q}\sigma\sigma'} V_{\mathbf{p}-\mathbf{p}'} c_{\mathbf{p}\sigma}^{\dagger} c_{\mathbf{p}'+\mathbf{q}\sigma'}^{\dagger} c_{\mathbf{p}+\mathbf{q}\sigma} c_{\mathbf{p}'\sigma'}, \quad (2)$$

where the uncorrelated spectrum of electrons with an account of long-range hoppings (with the intensity determined by parameters  $t_2$  and  $t_3$ ) is described by the expression

$$\varepsilon_{\mathbf{p}} = 2t_1(\cos p_x d + \cos p_y d) + 4t_2 \cos p_x d \cos p_y d + 2t_3(\cos 2p_x d + \cos 2p_y d). \quad (3)$$

The utilization of the weak-coupling Born approximation allows us to calculate the effective interaction for the Cooper channel by restricting ourselves to the diagrams of the first and second order in the bare interaction  $U_{\text{vac}}$ . In this case, the real small parameter of the problem is the parameter

$$U_{\text{vac}}(q=0)\rho(\mu) < 1, \quad (4)$$

where  $\rho(\mu)$  is the density of states at the Fermi level. Note that in [31], we considered the opposite strong-coupling limit  $U > V > W$ . In this case, an account of only the first- and second-order diagrams for the effective interaction  $\Gamma$  is justified only in the low-electron density limit  $n \ll 1$ , when the Galitsky–Bloom Fermi-gas expansion is valid [40, 41]. In this paper, as in [31], we calculate only the main component for  $T_c$ . Exact evaluation of the pre-exponential factor requires consideration of the third- and fourth-order diagrams [15]. At the same time, the use of the Born approximation in this paper allows us to consider arbitrary electron densities  $0 < n < 1$ .

### 3. EFFECTIVE INTERACTION OF ELECTRONS IN A COOPER CHANNEL

The second-order correction  $\delta\tilde{\Gamma}(p, k)$  for the effective interaction in a Cooper channel is determined by the four Kohn–Luttinger diagrams shown in Fig. 1. The presence of two solid lines without arrows in the diagram means the summation over the spin projection values. The scattering of electrons with identical spin projections is related to the intersite contribution only. If the interacting electrons have opposite spins, the scattering amplitude is determined by the sum of the Hubbard and intersite interactions. Therefore, in the case of the Hubbard repulsion alone, the first three Kohn–Luttinger diagrams are mutually cancelled out upon the summation in spin, and the correction  $\delta\tilde{\Gamma}(p, k)$  to the effective interaction is determined only by the last exchange diagram [1, 4, 5].

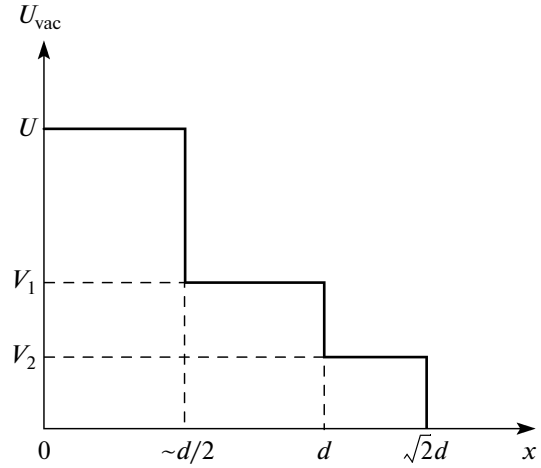


Fig. 2. The bare interaction in the Shubin–Vonsovsky model with Hubbard repulsion  $U$  and additional Coulomb repulsions  $V_1$  and  $V_2$  between electrons located at nearest and next-to-nearest sites.

When the Coulomb repulsion on neighboring sites is added, all diagrams in Fig. 1 contribute to the renormalized amplitude.

By relating the analytic expressions to the diagrams shown in Fig. 1, we find the second-order correction for the renormalized interaction,

$$\delta\tilde{\Gamma}^{(2)}(p, k) = -T \sum_{\mathbf{p}_1, i\omega_l} (U + V_{\mathbf{p}-\mathbf{k}}) \times (V_{\mathbf{p}_1+\mathbf{p}} - 2V_{\mathbf{p}-\mathbf{k}} + V_{\mathbf{p}_1-\mathbf{k}}) \times G_0(\mathbf{p}_1, i\omega_l) G_0(\mathbf{p}_1 + \mathbf{p} - \mathbf{k}, i\omega_l + i\omega_n - i\omega_m) \quad (5)$$

$$- T \sum_{\mathbf{p}_1, i\omega_l} (U + V_{\mathbf{p}_1-\mathbf{p}})(U + V_{\mathbf{p}_1-\mathbf{k}})$$

$$\times G_0(\mathbf{p}_1, i\omega_l) G_0(\mathbf{p}_1 - \mathbf{p} - \mathbf{k}, i\omega_l - i\omega_n - i\omega_m).$$

Summation over the Matsubara frequencies yields

$$\tilde{\Gamma}(p, k) = U + V_{\mathbf{p}-\mathbf{k}} + \delta\tilde{\Gamma}(p, k), \quad (6)$$

$$\delta\tilde{\Gamma}(p, k) = \frac{1}{N} \sum_{\mathbf{p}_1} (U + V_{\mathbf{p}-\mathbf{k}}) \times (2V_{\mathbf{p}-\mathbf{k}} - V_{\mathbf{p}_1+\mathbf{p}} - V_{\mathbf{p}_1-\mathbf{k}}) \times \frac{f(\varepsilon_{\mathbf{p}_1}) - f(\varepsilon_{\mathbf{p}_1+\mathbf{p}-\mathbf{k}})}{i\omega_n - i\omega_m + \varepsilon_{\mathbf{p}_1} - \varepsilon_{\mathbf{p}_1+\mathbf{p}-\mathbf{k}}} \quad (7)$$

$$+ \frac{1}{N} \sum_{\mathbf{p}_1} (U + V_{\mathbf{p}_1-\mathbf{p}})(U + V_{\mathbf{p}_1-\mathbf{k}}) \times \frac{f(\varepsilon_{\mathbf{p}_1}) - f(\varepsilon_{\mathbf{p}_1-\mathbf{p}-\mathbf{k}})}{i\omega_n + i\omega_m - \varepsilon_{\mathbf{p}_1} + \varepsilon_{\mathbf{p}_1-\mathbf{p}-\mathbf{k}}},$$

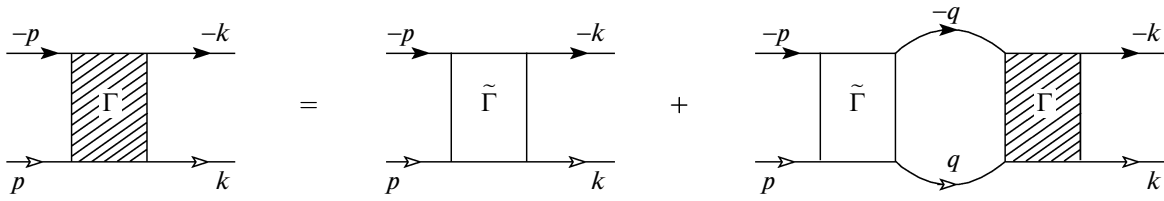


Fig. 3. Bethe–Salpeter integral equation for two electrons in the Cooper channel.

where  $f(x) = \{\exp[(x - \mu)/T] + 1\}^{-1}$  is the Fermi–Dirac distribution function. In expressions (5)–(7), the four-momenta and Matsubara frequencies are introduced,

$$p \equiv (\mathbf{p}, i\omega_n), \quad \omega_n = (2n + 1)\pi T, \quad n = 0, \pm 1, \dots,$$

$$k \equiv (\mathbf{k}, i\omega_m), \quad \omega_m = (2m + 1)\pi T, \quad m = 0, \pm 1, \dots$$

#### 4. BETHE–SALPETER INTEGRAL EQUATION

Knowledge of the renormalized expression for the effective interaction allows us to analyze the conditions for the realization of the Cooper instability in the model under study. To solve this problem, we will find, as usual, the total scattering amplitude  $\Gamma(p, k)$  of two electrons with opposite momenta and spin projection values (Cooper amplitude) and with the energies close to the Fermi energy. This amplitude in the ladder approximation satisfies the Bethe–Salpeter equation, in which the renormalized interaction  $\tilde{\Gamma}(p, k)$  (the irreducible vertex for the Cooper channel) serves as the “bare” interaction. The diagrammatic form of this equation is shown in Fig. 3. The Bethe–Salpeter integral equation in the analytic form is described by the expression

$$\Gamma(p, k) = \tilde{\Gamma}(p, k) + \frac{T}{N} \sum_q \tilde{\Gamma}(p, q) \frac{\Gamma(q, k)}{\omega_q^2 + \xi_q^2}, \quad (8)$$

where  $q \equiv (\mathbf{q}, \omega_q)$  and  $\xi_q = \varepsilon_q - \mu$ . The summation over intermediate Matsubara frequencies  $\omega_q$  is performed taking into account that the main contribution to the scattering amplitude  $\Gamma(p, k)$  is provided by the scattering of electrons with the energies close to the Fermi energy. This allows us to neglect the dependence of  $\tilde{\Gamma}$  in (8) on the Matsubara frequency. In this case, the total amplitude  $\Gamma(p, k)$  is also independent of Matsubara frequencies and the Bethe–Salpeter equation is simplified,

$$\Gamma(\mathbf{p}, \mathbf{k}) = \tilde{\Gamma}(\mathbf{p}, \mathbf{k}) - \frac{1}{N} \sum_q \tilde{\Gamma}(\mathbf{p}, \mathbf{q}) L(\xi_q) \Gamma(\mathbf{q}, \mathbf{k}), \quad (9)$$

where  $L(\xi_q) = \tanh(\xi_q/2T)/2\xi_q$  is a standard expression for the Cooper loop.

It is known [42] that the appearance of the Cooper instability can be found by analyzing the homogeneous part of Eq. (9). In this case, the dependence on

momentum  $\mathbf{k}$  is factorized and we can omit it in the further discussion. As a result, an integral equation for  $\Gamma(\mathbf{p}, \mathbf{k})$  or for the superconducting gap  $\Delta(\mathbf{p})$  appears. By passing to integration over isoenergetic contours (in the two-dimensional case), we find that the possibility of the Cooper pairing is determined by the characteristics of the energy spectrum in the vicinity of the Fermi level and by the renormalized interaction  $\tilde{\Gamma}(\mathbf{p}, \mathbf{k})$  of the electrons located near the Fermi surface  $\varepsilon_q = \mu$  [13, 16, 22, 24–26, 30]. As a result, analysis of the Cooper instability reduces to solving the eigenvalue problem

$$\frac{1}{(2\pi)^2} \oint_{\varepsilon_q = \mu} \frac{d\hat{\mathbf{q}}}{v_F(\hat{\mathbf{q}})} \tilde{\Gamma}(\hat{\mathbf{p}}, \hat{\mathbf{q}}) \Delta(\hat{\mathbf{q}}) = \lambda \Delta(\hat{\mathbf{p}}) \quad (10)$$

in which the superconducting order parameter  $\Delta(\hat{\mathbf{q}})$  plays the role of the eigenvector, and the eigenvalues satisfy the condition  $\lambda^{-1} \approx \ln(T_c/W)$ . In this case, quasi-momenta  $\hat{\mathbf{p}}$  and  $\hat{\mathbf{q}}$  are located on the Fermi surface and  $v_F(\hat{\mathbf{q}})$  is the Fermi velocity. One can see that the allowed solutions to Eq. (10) with  $\lambda < 0$  are determined not only by the effective interaction  $\tilde{\Gamma}(\mathbf{p}, \mathbf{q})$  but also by the shape of isoenergetic contours. Since the particular structure of these contours is closely related to the energy spectrum, it is obvious that the outcome beyond the nearest-neighbor approximation, when hoppings to the sites located in distant coordination spheres are taken into account, can substantially affect the conditions for the realization of the Cooper instability and noticeably modify the structure of the phase diagram of the superconducting state (see below).

To solve Eq. (10), we represent its kernel as a superposition of functions, each of them related to one of the irreducible representations of the symmetry group  $C_{4v}$  of a square lattice. This group has five irreducible representations [43], and Eq. (10) has for each of the representations its own solution with the corresponding effective coupling constant  $\lambda$ . Below, we will use the following classification for the symmetry of the order parameter: the representation  $A_1$  corresponds to the  $s$ -wave symmetry type,  $A_2$  to the extended  $s$ -wave symmetry ( $s_{\text{ext}}$ ),  $B_1$  to the  $d_{xy}$ -wave symmetry,  $B_2$  to the  $d_{x^2-y^2}$ -wave symmetry, and  $E$  to the  $p$ -wave symmetry.

The solution to Eq. (10) for the irreducible representation  $\alpha$  is sought in the form

$$\Delta^{(\alpha)}(\phi) = \sum_m \Delta_m^{(\alpha)} g_m^{(\alpha)}(\phi), \quad (11)$$

where  $m$  is the number of the basis function of the representation  $\alpha$ , and  $\phi$  is the angle characterizing the direction of momentum  $\hat{\mathbf{p}}$  with respect to the  $p_x$  axis. The explicit form of orthonormalized functions  $g_m^{(\alpha)}(\phi)$  is determined by the expressions

$$\begin{aligned} A_1 &\longrightarrow g_m^{(s)}(\phi) = \frac{1}{\sqrt{(1 + \delta_{m0})\pi}} \cos 4m\phi, \\ & \quad m \in [0, \infty), \\ A_2 &\longrightarrow g_m^{(s_{\text{ext}})}(\phi) = \frac{1}{\sqrt{\pi}} \sin 4(m+1)\phi, \\ B_1 &\longrightarrow g_m^{(d_{xy})}(\phi) = \frac{1}{\sqrt{\pi}} \sin(4m+2)\phi, \\ B_2 &\longrightarrow g_m^{(d_{x^2-y^2})}(\phi) = \frac{1}{\sqrt{\pi}} \cos(4m+2)\phi, \\ E &\longrightarrow g_m^{(p)}(\phi) = \frac{1}{\sqrt{\pi}} (A \sin(2m+1)\phi \\ & \quad + B \cos(2m+1)\phi). \end{aligned} \quad (12)$$

The basis functions satisfy the orthonormalization conditions

$$\int_0^{2\pi} d\phi g_m^{(\alpha)}(\phi) g_n^{(\beta)}(\phi) = \delta_{\alpha\beta} \delta_{mn}. \quad (13)$$

By substituting (11) into Eq. (10), performing the integration over angles, and using the orthonormalization condition for functions  $g_m^{(\alpha)}(\phi)$ , we obtain

$$\sum_n \Lambda_{mn}^{(\alpha)} \Delta_n^{(\alpha)} = \lambda_\alpha \Delta_m^{(\alpha)}, \quad (14)$$

where

$$\begin{aligned} \Lambda_{mn}^{(\alpha)} &= \frac{1}{(2\pi)^2} \int_0^{2\pi} d\phi_p \int_0^{2\pi} d\phi_q \frac{d\hat{\mathbf{q}}}{d\phi_q v_F(\hat{\mathbf{q}})} \tilde{\Gamma}(\mathbf{p}, \mathbf{q}) \\ & \quad \times g_m^{(\alpha)}(\phi_p) g_n^{(\alpha)}(\phi_q). \end{aligned} \quad (15)$$

Since  $T_c \sim W \exp(1/\lambda)$ , a superconducting phase with  $\alpha$  symmetry of the order parameter corresponds to each negative eigenvalue  $\lambda_\alpha$ . The expansion of the order parameter  $\Delta^{(\alpha)}(\phi)$  over the basis functions includes, generally speaking, a large number of harmonics, but the main contribution is determined by only a few terms (see below). The larger value of the critical temperature corresponds to the largest absolute value of  $\lambda_\alpha$ .

## 5. NUMERICAL CALCULATION

Equation (14) was solved numerically by dividing the Fermi contour into 300 intervals, while the Brillouin zone was divided into  $10^6$  squares with a linear size of  $2\pi 10^{-3}$ . It was found that this partition method was sufficient to describe correctly the dependence of the effective coupling constant  $\lambda$  on the electron density  $n$  [44]. Based on the dependences  $\lambda(n)$  found for different values of intersite Coulomb interactions  $V_1$  and  $V_2$ , we constructed the phase diagrams of the Shubin–Vonsovsky model reflecting the competition between superconducting phases with different symmetry types of the order parameter.

To conveniently present our results and demonstrate the relative contributions of different components of the effective interaction in first- and second-order perturbation theory to the development of Cooper instability, we represent the expression for  $\tilde{\Gamma}$  as the sum of four terms:

$$\begin{aligned} \tilde{\Gamma}(\mathbf{p}, \mathbf{q}) &= \tilde{\Gamma}_I(\mathbf{p}, \mathbf{q}) + \tilde{\Gamma}_{U^2}(\mathbf{p}, \mathbf{q}) \\ & \quad + \tilde{\Gamma}_{UV}(\mathbf{p}, \mathbf{q}) + \tilde{\Gamma}_{V^2}(\mathbf{p}, \mathbf{q}), \end{aligned} \quad (16)$$

where

$$\begin{aligned} \tilde{\Gamma}_I(\mathbf{p}, \mathbf{q}) &= U + V\gamma_{\mathbf{p}-\mathbf{q}} = U_{\text{vac}}(\mathbf{p}-\mathbf{q}), \\ \tilde{\Gamma}_{U^2}(\mathbf{p}, \mathbf{q}) &= \frac{U^2}{N} \sum_{\mathbf{p}_1} \chi_{\mathbf{p}_1-\mathbf{p}-\mathbf{q}}, \\ \tilde{\Gamma}_{UV}(\mathbf{p}, \mathbf{q}) &= \frac{UV_1}{N} \sum_{\mathbf{p}_1} ((2\gamma_{\mathbf{p}-\mathbf{q}} - \gamma_{\mathbf{p}_1+\mathbf{p}} - \gamma_{\mathbf{p}_1-\mathbf{q}}) \chi_{\mathbf{p}_1+\mathbf{p}-\mathbf{q}} \\ & \quad + (\gamma_{\mathbf{p}_1-\mathbf{q}} + \gamma_{\mathbf{p}_1-\mathbf{p}}) \chi_{\mathbf{p}_1-\mathbf{p}-\mathbf{q}}), \\ \tilde{\Gamma}_{V^2}(\mathbf{p}, \mathbf{q}) &= \frac{V_1^2}{N} \sum_{\mathbf{p}_1} (\gamma_{\mathbf{p}-\mathbf{q}} (2\gamma_{\mathbf{p}-\mathbf{q}} - \gamma_{\mathbf{p}_1+\mathbf{p}} - \gamma_{\mathbf{p}_1-\mathbf{q}}) \chi_{\mathbf{p}_1+\mathbf{p}-\mathbf{q}} \\ & \quad + \gamma_{\mathbf{p}_1-\mathbf{q}} \gamma_{\mathbf{p}_1-\mathbf{p}} \chi_{\mathbf{p}_1-\mathbf{p}-\mathbf{q}}). \end{aligned}$$

The functions of momenta entering these expressions have the form

$$\begin{aligned} \gamma_{\mathbf{p}-\mathbf{q}} &= 2[\cos(p_x - q_x)d + \cos(p_y - q_y)d] \\ & \quad + 4v \cos(p_x - q_x)d \cos(p_y - q_y)d, \end{aligned} \quad (17)$$

where  $v = V_2/V_1$ , and the generalized susceptibilities (polarization loops) have the form

$$\chi_{\mathbf{p}_1 \pm \mathbf{p} - \mathbf{q}} = \frac{f(\epsilon_{\mathbf{p}_1}) - f(\epsilon_{\mathbf{p}_1 \pm \mathbf{p} - \mathbf{q}})}{\mp(\epsilon_{\mathbf{p}_1 \pm \mathbf{p} - \mathbf{q}} - \epsilon_{\mathbf{p}_1})}. \quad (18)$$

Since the first-order perturbation theory in the intersite Coulomb interaction always tends to suppress the superconductive pairing, the possibility of obtaining the Cooper instability based on the Kohn–Luttinger mechanism is attributed to the appearance (in

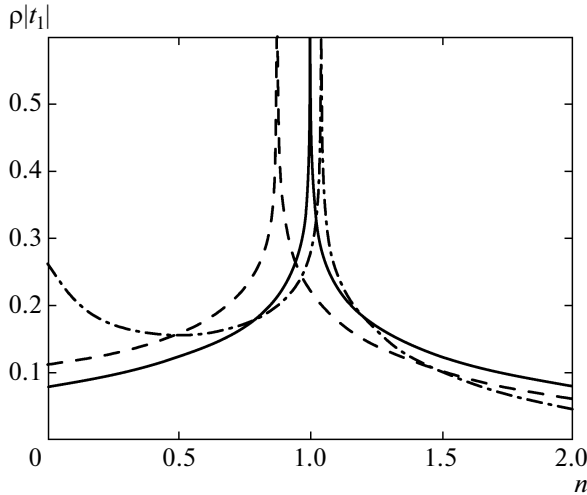


**Fig. 4.** Density of electron states calculated for sets of parameters  $t_2 = t_3 = 0$  (solid curve),  $t_2 = 0.15|t_1|$ ,  $t_3 = 0$  (dashed curve), and  $t_2 = 0.15|t_1|$ ,  $t_3 = 0.10|t_1|$  (dash-and-dot curve).

the second-order perturbation theory) of the contributions to the matrix of the effective interaction for the Cooper channel (15), (16), which correspond to the attraction and have a sufficiently high intensity. The conditions required to achieve the superconducting phase with the specified symmetry of the order parameter  $\Delta^{(\alpha)}(\phi)$  can be obtained by analyzing the matrix elements of the effective interaction  $\tilde{\Gamma}$  for the same symmetry type. By analyzing each partial contribution in the similar manner, we can also determine the main second-order terms for the effective interaction in (16) that produces the Cooper pairing. For this purpose, we will write the resulting effective interaction  $\tilde{\Gamma}$  for each irreducible representation  $\alpha$  as the sum of the matrix elements in the representation of the basis functions (12):

$$\begin{aligned} \{\tilde{\Gamma}^{(\alpha)}\}_{mn} &= \{\tilde{\Gamma}_I^{(\alpha)}\}_{mn} + \{\tilde{\Gamma}_{U^2}^{(\alpha)}\}_{mn} \\ &+ \{\tilde{\Gamma}_{UV}^{(\alpha)}\}_{mn} + \{\tilde{\Gamma}_{V^2}^{(\alpha)}\}_{mn}, \end{aligned} \quad (19)$$

where

$$\begin{aligned} \{\tilde{\Gamma}_I^{(\alpha)}\}_{mn} &= \frac{1}{(2\pi)^2} \int_0^{2\pi} d\phi_p \int_0^{2\pi} d\phi_q \tilde{\Gamma}_I(\hat{\mathbf{p}}, \hat{\mathbf{q}}) \\ &\times g_m^{(\alpha)}(\phi_p) g_n^{(\alpha)}(\phi_q), \end{aligned} \quad (20)$$

$$\begin{aligned} \{\tilde{\Gamma}_{U^2}^{(\alpha)}\}_{mn} &= \frac{1}{(2\pi)^2} \int_0^{2\pi} d\phi_p \int_0^{2\pi} d\phi_q \tilde{\Gamma}_{U^2}(\hat{\mathbf{p}}, \hat{\mathbf{q}}) \\ &\times g_m^{(\alpha)}(\phi_p) g_n^{(\alpha)}(\phi_q), \end{aligned} \quad (21)$$

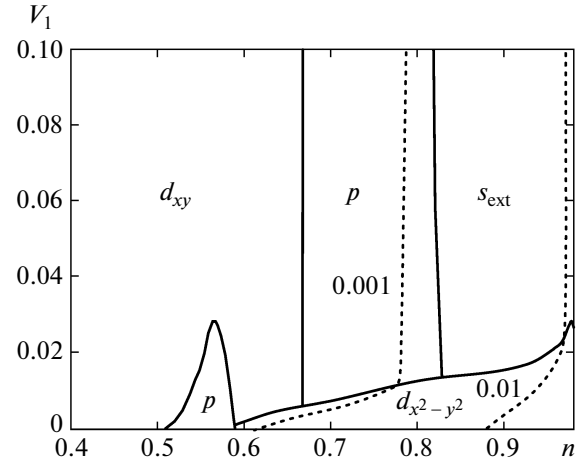


**Fig. 5.** Phase diagram of the Shubin–Vonsovsky model in  $n$ – $V_1$  variables for  $t_1 = -1$ ,  $t_2 = t_3 = 0$ ,  $U = |t_1|$  and  $V_2/V_1 = 0$ . Intersite Coulomb interaction is taken into account only in first order of perturbation theory. For all points belonging to one dashed line, the value of  $\lambda$  is constant and indicated by a corresponding number.

$$\begin{aligned} \{\tilde{\Gamma}_{UV}^{(\alpha)}\}_{mn} &= \frac{1}{(2\pi)^2} \int_0^{2\pi} d\phi_p \int_0^{2\pi} d\phi_q \tilde{\Gamma}_{UV}(\hat{\mathbf{p}}, \hat{\mathbf{q}}) \\ &\times g_m^{(\alpha)}(\phi_p) g_n^{(\alpha)}(\phi_q), \end{aligned} \quad (22)$$

$$\begin{aligned} \{\tilde{\Gamma}_{V^2}^{(\alpha)}\}_{mn} &= \frac{1}{(2\pi)^2} \int_0^{2\pi} d\phi_p \int_0^{2\pi} d\phi_q \tilde{\Gamma}_{V^2}(\hat{\mathbf{p}}, \hat{\mathbf{q}}) \\ &\times g_m^{(\alpha)}(\phi_p) g_n^{(\alpha)}(\phi_q). \end{aligned} \quad (23)$$

As mentioned above, the inclusion of long-range electron hoppings is also important, which can shift the van Hove singularity in the density of states from the half-filling ( $n = 1$ ) to the region of the lower (or higher) electron densities (Fig. 4). In this paper, to avoid the summation of parquet diagrams [45], we analyzed the concentration dependences of the effective coupling constants only for electron densities not very close to the van Hove singularity, for which  $U_{\text{vac}}(q=0)\rho(\mu) < 1$ .

## 6. PHASE DIAGRAM OF THE SHUBIN–VONSOVSKY MODEL

### 6.1. First Order in $V$

If the intersite Coulomb interaction is taken into account only for the electrons located at nearest sites ( $V_1 \neq 0$ ,  $V_2 = 0$ ) and the excitation spectrum is described by one hopping parameter ( $t_1 \neq 0$ ,  $t_2 = t_3 = 0$ ), then for  $U = |t_1|$ , the phase diagram of the superconducting states contains five regions (Fig. 5). This diagram was obtained by taking into account only

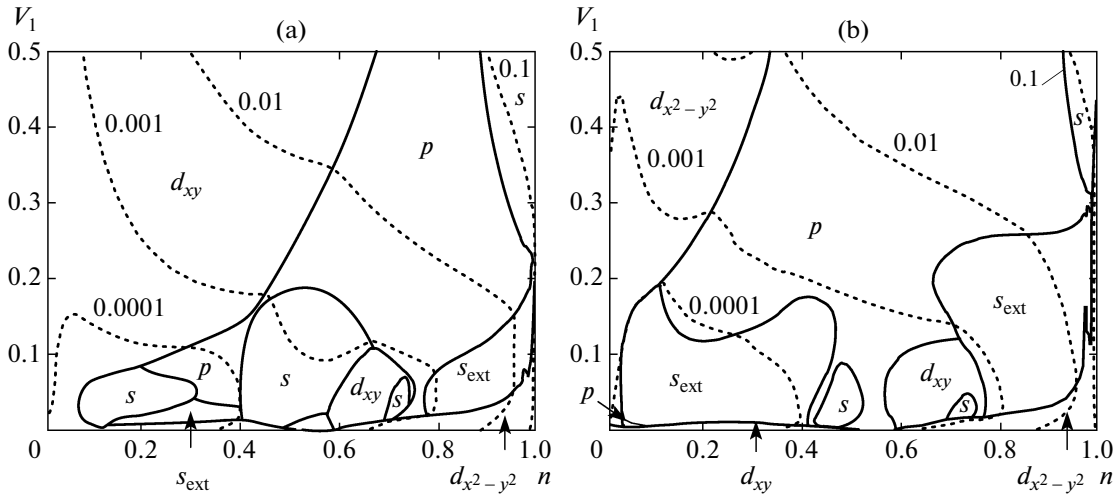


**Fig. 6.** Phase diagrams of the Shubin–Vonsosky model in  $n$ – $V_1$  variables constructed taking into account second-order contributions in  $V$  for set of parameters  $t_1 = -1$ ,  $t_2 = t_3 = 0$ ,  $U = |t_1|$  and  $V_2/V_1 = 0$  (a) and 0.5 (b). Dotted curves correspond to constant  $\lambda$  values.

first-order contributions in  $V$  in the expression for the effective interaction of electrons in the Cooper channel,

$$\tilde{\Gamma}(\mathbf{p}, \mathbf{q}) = \tilde{\Gamma}_I(\mathbf{p}, \mathbf{q}) + \tilde{\Gamma}_{V^2}(\mathbf{p}, \mathbf{q}), \quad (24)$$

and neglecting contributions proportional to  $UV$  and  $V^2$ .

The parts of the phase diagram lying on the abscissa ( $V_1 = 0$ ) agree well with regions in the phase diagram obtained in [24]. In the region of low electron densities  $n = 0$ – $0.52$  in the first two orders of the perturbation theory, superconductivity with the  $d_{xy}$ -wave symmetry of the order parameter is achieved in [13, 16]; in the interval  $n = 0.52$ – $0.58$ , the phase with  $p$ -wave pairing corresponds to the ground state, but the absolute value of  $\lambda_p$  slightly exceeds  $\lambda_{d_{xy}}$ . For  $n > 0.58$ , superconductivity of the  $d_{x^2-y^2}$ -wave type appears.

Note that an account of the Coulomb interaction  $V_1$  of electrons located at neighboring sites in the first-order perturbation theory leads to a decrease in the absolute value of  $\lambda$  for all symmetry types. In this case, the superconducting  $d_{x^2-y^2}$ -wave phase is more strongly suppressed, and as  $V_1$  increases, the phases with other symmetry types of the order parameter appear at the same concentrations.

### 6.2. Phase Diagram Taking into Account Second-Order Contributions in $V$

As mentioned above, polarization effects are manifested through second-order contributions in  $V$  to the effective interaction of electrons in the Cooper channel. Therefore, to account for Kohn–Luttinger effects connected with the intersite Coulomb interaction, it is necessary to use total expression (16) rather than trun-

cated expression (24) for  $\tilde{\Gamma}(\mathbf{p}, \mathbf{q})$ . In this case, polarization effects, proportional to  $UV$  and  $V^2$ , considerably change and complicate the structure of the phase diagram even for small  $V_1$  (Fig. 6a). In particular, for  $V_1/|t_1| = 0$ – $0.2$ , a strong competition between the  $d_{xy}$ -,  $p$ -,  $s$ -, and  $s_{ext}$ -wave superconductivity types takes place in the entire region of electron densities. The result of this competition can be determined by comparing small values of the effective coupling constant  $\lambda$ . This is demonstrated in Fig. 6 where the dashed curves correspond the constant  $\lambda$  values. As the intersite Coulomb interaction parameter  $V_1$  is increased, the absolute value of  $\lambda$  increases. In this case, only three phases corresponding to the  $d_{xy}$ -,  $p$ -, and  $s$ -wave symmetry types of the superconducting order parameter are stabilized. Note that in the region of high electron concentrations and for  $V_1/|t_1| = 0.25$ – $0.5$ , the polarization Kohn–Luttinger effects give rise to the superconducting  $s$ -wave phase. This qualitative effect clearly demonstrates the importance of the second-order effects when calculating the effective interaction of electrons in the Cooper channel and constructing the complicated phase diagram in Fig. 6.

Let us quantitatively compare the different partial contributions to the total effective interaction and demonstrate the significant role of the second-order in  $V$  contributions to  $\tilde{\Gamma}$ . Matrix elements  $\{\tilde{\Gamma}\}_{mn}$  (20)–(23) calculated for small  $m$  and  $n$  are presented below in the table. The values of the matrix elements for  $n$ ,  $m > 2$  are not given because of their smallness. The table reflects the results for a point of the phase diagram in which the superconducting phase with the  $s$ -wave symmetry of the order parameter corresponds to the ground state. One can see from the table that, for

The values of the matrix element for partial contributions  $\{\tilde{\Gamma}_I^{(s)}\}_{mn}$ ,  $\{\tilde{\Gamma}_{V^2}^{(s)}\}_{mn}$ ,  $\{\tilde{\Gamma}_{UV}^{(s)}\}_{mn}$ ,  $\{\tilde{\Gamma}_{V^2}^{(s)}\}_{mn}$ , and the resulting effective interaction  $\{\tilde{\Gamma}^{(s)}\}_{mn}$  and the values of the expansion coefficients of the order parameter  $\Delta_m^{(s)}$ . Calculations were performed for parameters  $t_1 = -1$ ,  $t_2 = t_3 = 0$ ,  $U = |t_1|$ ,  $V_1 = 0.5|t_1|$ ,  $V_2 = 0$ , and  $n = 0.95$

$(m, n)$	(0, 0)	(1, 1)	(1, 0)	(2, 2)	(2, 1)	(2, 0)
$\{\tilde{\Gamma}_I^{(s)}\}_{mn}$	6.288	0	0.001	0	0	0.001
$\{\tilde{\Gamma}_{V^2}^{(s)}\}_{mn}$	1.972	0.106	0.058	0.036	0.006	0.030
$\{\tilde{\Gamma}_{UV}^{(s)}\}_{mn}$	1.758	0.763	-0.245	0.214	0.136	-0.090
$\{\tilde{\Gamma}_{V^2}^{(s)}\}_{mn}$	-6.589	-3.684	-0.324	-0.481	-0.494	-0.111
$\{\tilde{\Gamma}^{(s)}\}_{mn}$	3.429	-2.815	-0.509	-0.231	-0.353	-0.170
$m$	0	1	2	3	4	5
$\Delta_m^{(s)}$	-0.188	0.968	0.163	0.039	0.010	0.003

the chosen parameters, the first- and second-order contributions  $\tilde{\Gamma}_I$  and  $\tilde{\Gamma}_{V^2}$ , respectively, give only positive values of the matrix elements. This means that an account of only these processes would not lead to the superconducting phase with the  $s$ -wave symmetry of the order parameter. Similarly, the second-order contributions  $\tilde{\Gamma}_{UV}$  would not give rise to the superconducting  $s$ -wave phase either, and only the second-order contributions  $\tilde{\Gamma}_{V^2}$  (the fourth line of the table) provide the negative values of the matrix elements  $\{\tilde{\Gamma}\}_{mn}$  (and thereby negative eigenvalues  $\lambda$ ) leading to the realization of the superconducting  $s$ -wave phase. Note that the main contribution to the angular dependence of the superconducting order parameter is made by the harmonic  $g_1^{(s)}(\phi) = (1/\sqrt{\pi})\cos 4\phi$  (the last line in the table). It should be pointed out in this connection that, despite the large value of the matrix element  $\{\tilde{\Gamma}_{V^2}^{(s)}\}_{00}$  for  $g_0^{(s)}(\phi) = 1/\sqrt{2\pi}$ , other partial contributions suppress the tendency toward superconductivity in a channel with the absence of the angular dependence of the order parameter ( $\Delta_0^{(s)} \sim g_0^{(s)} = \text{const}$ ).

Let us comment on the values of  $\Delta_m^{(s)}$  in the table. We determined the Cooper instability by analyzing the homogeneous part of the Bethe–Salpeter equation. It is known that in this case the order parameter is determined with an accuracy of the common factor  $\Delta$ , which is proportional to  $\sqrt{(T_c - T)/T_c}$  in the vicinity of the critical point  $T < T_c$  in the weak coupling case (the BCS model). Therefore, the values in the table reflect only the relative contribution of each harmonic to the angular dependence of the order parameter.

This scenario of achieving superconducting  $s$ -wave pairing due to higher harmonics correlates well with recent experimental data obtained in [46], where an iron arsenide superconductor  $\text{KFe}_2\text{As}_2$  was studied by photoemission spectroscopy with ultrahigh angular resolution. These investigations have shown that this compound is a nodal (containing zeroes of the gap) superconductor with  $s$ -wave symmetry of the order parameter, which has eight points at which the gap vanishes.

For comparison, Fig. 7 shows the results of our calculation performed for the point of the phase diagram discussed above in which the superconducting phase with  $s$ -wave symmetry of the order parameter corresponds to the ground state at high electron densities. The expansion of the order parameter  $\Delta_3^{(s)}$  in angular harmonics in this case is described by the expression

$$\Delta^{(s)}(\phi) = \frac{\Delta_0^{(s)}}{\sqrt{2}} + \Delta_1^{(s)}\cos 4\phi + \Delta_2^{(s)}\cos 8\phi + \Delta_3^{(s)}\cos 12\phi + \Delta_4^{(s)}\cos 16\phi \quad (25)$$

with coefficients  $\Delta_m^{(s)}$  given in the last line of the table.

Note that, starting from  $\Delta_3^{(s)}$ , the expansion coefficients are small, so that the gap is described well by the first three terms. Figure 7a shows the corresponding angular dependence of the superconducting order parameter  $\Delta^{(s)}(\phi)$ , which demonstrates the presence of the eight nodal points at which the gap vanishes. Note that the arrangement of nodal points of  $\Delta^{(s)}(\phi)$  on the Fermi contour (Fig. 7b) in our calculation qualitatively agrees with the picture presented in [46].

The scenario of realization of the superconductivity, which resembles the scenario of the appearance of

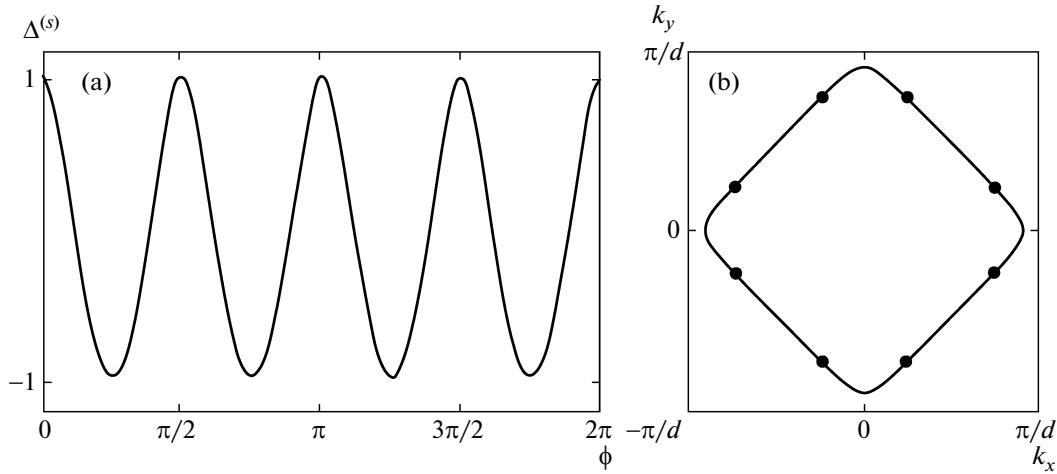


**Fig. 7.** Angular dependence of the superconducting order parameter  $\Delta^{(s)}(\phi)$  (a) and location of the nodal points at which the gap  $\Delta^{(s)}(\phi)$  vanishes on the Fermi contour (b), calculated for the parameters  $t_1 = -1$ ,  $t_2 = t_3 = 0$ ,  $U = |t_1|$ ,  $V_1 = 0.5|t_1|$ ,  $V_2 = 0$ , and  $n = 0.95$ .

$s$ -wave pairing, is also observed in the  $p$ -wave channel: the superconductivity realized in the second-order of the perturbation theory in the Coulomb interaction is suppressed by the bare repulsion  $\tilde{\Gamma}_I$  only for the first harmonic  $g_0^{(p)}$ . The main contribution to  $\Delta^{(p)}(\hat{\mathbf{p}})$  is introduced by the function of the next harmonic of  $p$ -wave pairing  $g_1^{(p)}(\phi) = (1/\sqrt{\pi})(A\sin 3\phi + B\cos 3\phi)$ .

The inclusion of the intersite Coulomb interaction  $V_2$  of the electrons from the second coordination sphere considerably modifies the phase diagram of the Shubin–Vonsovsky model. This is demonstrated by the phase diagrams in Fig. 6b, which are constructed for the ratio  $V_2/V_1 = 0.5$ , while the other parameters are not changed. For small  $V_1$  values, the phase diagram considerably changes (remaining complex, as in Fig. 6a); however, the effective interaction constant  $\lambda$  in this region is still small. For this reason, we will not consider in detail the region of small  $V_1$ . For large  $V_1$  values, the region in which  $p$ -wave pairing is realized expands, while in the region of low electron densities,  $d_{x^2-y^2}$ -wave pairing is realized instead of the  $d_{xy}$ -wave phase for the order parameter.

Note that in the region of high electron densities ( $n > 0.6$ ) and small  $V_1$ , the main contribution to  $d_{x^2-y^2}$ -wave Cooper pairing is introduced by the  $\tilde{\Gamma}_{V^2}$  matrix. As the parameter  $V_1$  increases, this contribution is sup-

pressed by the bare interaction  $\tilde{\Gamma}_I^{(d_{x^2-y^2})}$ . Meanwhile, the superconducting contribution begins to increase.

This contribution is caused by the  $\tilde{\Gamma}_{UV}^{(d_{x^2-y^2})}$  matrix with

the second  $d$ -pairing harmonic  $g_1^{(d_{x^2-y^2})}(\phi) = (1/\sqrt{\pi})\cos 6\phi$ , but the corresponding value of the coupling constant  $\lambda$  is still comparatively small. For this reason, an account of the interactions proportional to  $V_2$  weakly changes this region of the phase diagram.

In the case when  $V_1 \neq 0$  and  $V_2 \neq 0$ , the contribution to the  $d_{x^2-y^2}$ -wave pairing in the region of low concentrations is completely induced by the  $\tilde{\Gamma}_{V^2}$  matrix with the dominant role of the first  $d$ -wave pairing harmonic  $g_0^{(d_{x^2-y^2})}(\phi) = (1/\sqrt{\pi})\cos 2\phi$ . This contribution exceeds the bare repulsion contribution.

The competition between different superconducting phases is considerably affected by the inclusion of the electron hoppings to sites located beyond the first coordination sphere. This is demonstrated in Fig. 8, which shows the phase diagram of the model obtained for the values of parameters  $U = |t_1|$  and  $V_2/V_1 = 0.5$  taking into account electron hoppings within the first two coordination spheres ( $t_2 = 0.15|t_1|$  and  $t_3 = 0$ ). For this set of electron-hopping parameters, the critical electron density  $n_{vH}$  at which the van Hove singularity is realized shifts from the half-filling region ( $n_{vH} = 1$ ) to the region of lower electron densities (see Fig. 4). By comparing Figs. 6b and 8, we see that the inclusion of the hopping integral  $t_2$  leads to the expansion of the region of  $d_{x^2-y^2}$ -wave pairing at low electron densities and to an increase in the absolute values of  $\lambda$  in this region. (We have shown that the effective interaction constant  $\lambda$  in the region of small  $V_1$  are negligibly small.

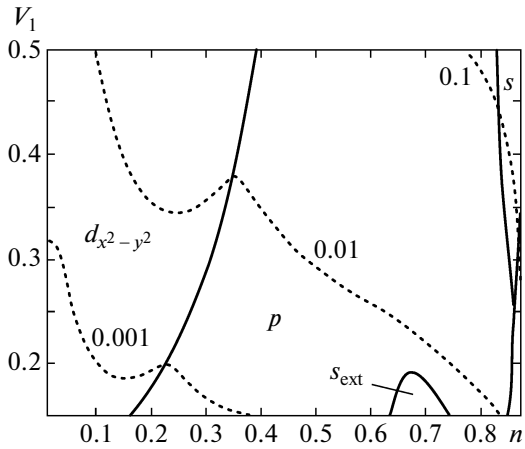


**Fig. 8.** Phase diagram of the Shubin–Vonsovsky model in  $n-V_1$  variables constructed for  $U = |t_1|$  and  $V_2/V_1 = 0.5$  for electron hopping parameters  $t_1 = -1$ ,  $t_2 = 0.15|t_1|$ , and  $t_3 = 0$ . Dotted curves correspond to constant  $\lambda$  values.

Therefore, further on, the phase diagrams of the model are constructed for  $V_1$  intervals with large  $\lambda$ ).

Note that for larger  $V_1$  values ( $V_1 \geq 0.2|t_1|$ ), the phase diagrams in Figs. 6 and 8 are significantly simplified.

Figure 9 shows the phase diagram calculated by additionally including electron hoppings to the third coordination sphere. By comparing phase diagrams in Figs. 8 and 9, we see that the inclusion of the hopping integral  $t_3 > 0$  leads to an increase in the effective interaction at low electron densities and to the additional

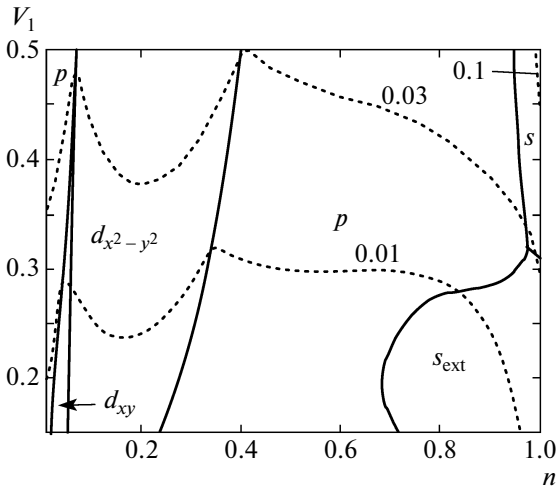


**Fig. 9.** Phase diagram of the Shubin–Vonsovsky model in  $n-V_1$  variables constructed for  $U = |t_1|$  and  $V_2/V_1 = 0.5$  for electron hopping parameters  $t_1 = -1$ ,  $t_2 = 0.15|t_1|$ , and  $t_3 = 0.1|t_1|$ . Dotted curves correspond to constant  $\lambda$  values.

expansion of the  $d_{x^2-y^2}$ -wave pairing region. Note that the inclusion of the hopping integral  $t_3 < 0$  results in the opposite effect.

We emphasize that in Section 6.1 we took into account Kohn–Luttinger corrections for the effective interaction that are only proportional to  $\tilde{\Gamma}_{U^2}$ . In this case, the phase diagram depends on only one parameter  $VW/U^2$ . However, when the contributions  $\tilde{\Gamma}_{UV}$  and  $\tilde{\Gamma}_{V^2}$  are taken into account, the dependence of the phase diagram on the Coulomb interaction parameters again becomes more complicated even for not too small values of  $V_1$ . Figure 10 shows the modification of the phase diagram of the Shubin–Vonsovsky model that occurs with an increase in Hubbard repulsion parameter  $U$ . The calculations were performed for the set of parameters  $t_2 = 0.15|t_1|$ ,  $t_3 = 0.1|t_1|$ , and  $V_2/V_1 = 0.5$ , as in Fig. 9, but for  $U = 2|t_1|$ . One can see that at low electron densities and at electron densities close to the van Hove singularity, the  $d_{x^2-y^2}$ -wave superconducting phase with sufficiently large values  $|\lambda| \sim 0.1-0.2$  is realized. This result seems important for studying the possibility of implementing the Kohn–Luttinger mechanism to high-temperature superconductors. Note that for  $|\lambda| \approx 0.2$ , the critical superconducting temperatures can reach realistic values  $T_c \sim 100$  K.

### 7. DISCUSSION

The results of the investigation of the Kohn–Luttinger mechanism of superconductivity and the char-

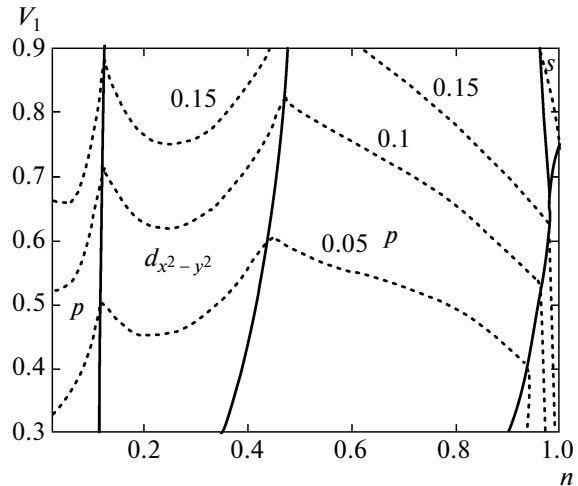


**Fig. 10.** Phase diagram of the Shubin–Vonsovsky model in  $n-V_1$  variables constructed for parameters  $t_1 = -1$ ,  $t_2 = 0.15|t_1|$ ,  $t_3 = 0.1|t_1|$ ,  $U = 2|t_1|$ , and  $V_2/V_1 = 0.5$ . Dotted curves correspond to constant  $\lambda$  values.

acter of the superconducting phase diagram in the Shubin–Vonsovsky model demonstrate a number of qualitatively new effects.

The first one is that the consideration of the second-order contributions of the perturbation theory in intersite Coulomb interaction  $V$  in the weak-coupling regime  $W > U > V$  leads to significant renormalization of the effective interaction for two electrons in the Cooper channel. Such a renormalization is related to the polarization Kohn–Luttinger effects, resulting in effective attraction of electrons in different channels on a two-dimensional square lattice. Note that the bare Coulomb interaction  $V$  always tends to suppress the Cooper pairing, whereas the second-order polarization effects in  $V$  facilitate an effective attraction. The main result is that the bare interaction suppresses superconductivity in some channels (in channels with some angular functions), whereas the second-order Kohn–Luttinger contributions generate superconductivity in the channels with other angular functions. Therefore, despite their parametric smallness, the second-order effects in  $V$  make the decisive contribution to the superconductivity mechanism in the Shubin–Vonsovsky model [39, 44].

The second effect is related to the modification of the phase diagram of the superconducting phase caused by the inclusion of the Coulomb interaction. In the absence of Coulomb interaction ( $V_1 = 0$ ,  $V_2 = 0$ ), the phase diagram of the 2D Hubbard model is quite simple and contains only three regions of the  $p$ -,  $d_{xy}$ -, and  $d_{x^2-y^2}$ -wave pairing [44] at different electron densities  $0 < n < 1$ . When the first-order contributions in the Coulomb interaction  $V_1$  at neighboring sites are taken into account, the phase diagram of the superconducting state in the Shubin–Vonsovsky model is only slightly complicated. The three pairing types mentioned above are supplemented with another extended  $s$ -wave pairing ( $s_{\text{ext}}$ -wave), while the phase diagram itself contains five regions (two  $p$ -wave pairing regions and  $d_{xy}$ -,  $d_{x^2-y^2}$ -, and  $s_{\text{ext}}$ -wave pairing regions).

However, when the second-order contributions in the Coulomb interaction at nearest sites ( $V_1$ ) and next-to-nearest sites ( $V_2$ ) are taken into account, the superconducting phase diagram becomes much more complicated and contains more than ten regions with different pairing types  $s$ -,  $s_{\text{ext}}$ -,  $p$ -,  $d_{xy}$ -, and  $d_{x^2-y^2}$ -wave. The phase diagram is especially complex for small  $V_1$  (Fig. 6). For larger  $V_1$  values, the phase diagram is again simplified (see Figs. 8 and 9). Nevertheless, as  $V_1$  increases, the presence of the regions with anomalous  $s$ -wave pairing  $\Delta^{(s)}(\phi) \sim \Delta_1^{(s)} \cos 4\phi$  at high electron densities  $n \rightarrow 1$  in the diagram becomes typical. Note that such an angular dependence of the superconducting gap with eight points on the Fermi surface where the gap vanishes (Fig. 7) agrees well with recent exper-

imental results obtained by ARPES for one family of superconductors based on iron arsenide  $\text{KFe}_2\text{As}_2$  [46].

Note also that the inclusion of the long-range hoppings ( $t_2 \neq 0$ ,  $t_3 \neq 0$ ) shifts the van Hove singularity in the density of states from the half-filling  $n_{vH} = 1$  to the region of lower (or higher) electron densities and, generally speaking, substantially changes the Fermi contour and the Fermi velocity  $v_F$  on the contour. Nevertheless, this inclusion does not drastically change the phase diagram for large  $V_1$  values, retaining the dominant role of the  $d_{x^2-y^2}$ -,  $p$ -, and anomalous  $s$ -wave pairing regions for  $V_1 \gtrsim 0.3|t_1|$  (see Figs. 8, 9) and typical critical temperature values (coupling constants  $\lambda$  in the different channels).

The final, and quite important, effect is manifested in the strong expansion of the region of the realization of the  $d_{x^2-y^2}$ -wave superconducting phase with increasing Hubbard repulsion parameter  $U$  (Fig. 10), and for  $U/|t_1| = 2-3$ , near the half-filling  $n \rightarrow 1$ , the critical temperature can reach realistic values of  $T_c \sim 100$  K. This result is of special interest because it opens a realistic way for using the Kohn–Luttinger mechanism in high-temperature superconductivity.

A more detailed analysis of the phase diagram of the superconducting state at temperatures below  $T_c$  requires the construction of the functional of the Ginzburg–Landau free energy and determination of all of its local and global extrema taking into account strong-coupling corrections [47, 48] to the fourth (in the order parameter  $\Delta$ ) terms and calculation of the pre-exponential factor (consideration of the third- and fourth-order diagrams) for  $T_c$  [8, 15, 28]. In this case, the situation can arise in which, at least before taking into account strong-coupling corrections, the free energy values corresponding to some local minima of the Ginzburg–Landau functional can be very close to each other. Thus, for some types of crystal lattice, the phases, for example, with  $d_{xy}$ - and  $d_{x^2-y^2}$ -wave symmetries of the order parameter can be strongly bound [28, 49]. As a result, when the strong-coupling corrections are taken into account, then near  $T_c$  (or for the second phase transition inside the superconducting phase at  $\tilde{T}_c < T_c$ ), the states with the superposition of the two order parameters for the  $p$ - or  $d$ -wave pairing (of the  $A\Delta_{xy} + B\Delta_{x^2-y^2}$  type) can appear in principle. In particular (see discussion in [28]), of interest is the possibility of getting the  $p + ip$  or  $d + id$  chiral state, when one of the coefficients,  $A$  or  $B$ , in this superposition is imaginary. It was shown experimentally that the  $p_x + ip_y$  chiral state with  $p$ -wave symmetry of the order parameter was obtained in the anisotropic superconducting  $A$  phase in  ${}^3\text{He}$  [8–10] and probably in superconducting ruthenates  $\text{Sr}_2\text{RuO}_4$  [50, 51].

Note in conclusion that the development of the Kohn–Luttinger ideology in the strong-coupling regime for nearly half-filling is one of the most urgent directions in the theory of superconductivity in strongly correlated electron systems. However, the solution of this problem requires consideration of strong intersite correlations in all orders of the perturbation theory. In this case, however, intersite correlations should be described taking into account the second-order contributions. One of the scenarios of construction of the theory in this direction involves atomic representation [52]. The actual models in which Kohn–Luttinger renormalizations can be included are the  $t$ – $J$  model [53–56] and the generalized  $t$ – $J$ – $V$  model [57], which represent effective low-energy variants of the Shubin–Vonsovsky model.

#### ACKNOWLEDGMENTS

The authors are grateful to A.S. Aleksandrov<sup>†</sup>, D.V. Efremov, V.V. Kabanov, Yu.V. Kopaev<sup>†</sup>, K.I. Kugel, M.S. Mar’enko, N.M. Plakida, and A.V. Chubukov for numerous discussions and constant attention to this work. The work was supported by the program “Quantum Mesoscopic and Disordered Structures, 20.7 of the Presidium of the RAS, the Russian Foundation for Basic Research (project nos. 11-02-00741 and 12-02-31130), the federal target program “Human Resources in Science and Education for Innovative Russia 2009–2013” (GK no. 16.740.11.0644), and a grant from the President of the Russian Federation (no. MK-526.2013.2). One of the authors (M.M.K.) thanks the Dynasty Foundation for support.

#### REFERENCES

- W. Kohn and J. M. Luttinger, *Phys. Rev. Lett.* **15**, 524 (1965).
- W. Kohn, *Phys. Rev. Lett.* **2**, 393 (1959); E. J. Woll, Jr. and W. Kohn, *Phys. Rev.* **126**, 1693 (1962).
- J. Friedel, *Adv. Phys.* **3**, 446 (1954); J. Friedel, *Nuovo Cimento, Suppl.* **2**, 287 (1958).
- D. Fay and A. Layzer, *Phys. Rev. Lett.* **20**, 187 (1968).
- M. Yu. Kagan and A. V. Chubukov, *JETP Lett.* **47**(10), 614 (1988); M. Yu. Kagan and A. V. Chubukov, *JETP Lett.* **50**(11), 517 (1989).
- M. A. Baranov, M. Yu. Kagan, and Yu. Kagan, *JETP Lett.* **64** (4), 301 (1996).
- M. Yu. Kagan, *Phys.—Usp.* **37**(1), 69 (1994).
- D. Vollhardt and P. Woelfle, *The Superfluid Phases of Helium 3* (Taylor and Francis, London, 1990).
- G. E. Volovik, *Exotic Properties of Superfluid <sup>3</sup>He* (World Scientific, Singapore, 1992).
- G. E. Volovik, *The Universe in a Helium Droplet* (Clarendon Press, Oxford, 2003).
- N. B. Kopnin, T. T. Heikkilä, and G. E. Volovik, *Phys. Rev. B* **83**, 220503(R) (2011).
- A. V. Chubukov and M. Yu. Kagan, *J. Phys.: Condens. Matter* **1**, 3135 (1989).
- M. A. Baranov, A. V. Chubukov, and M. Yu. Kagan, *Int. J. Mod. Phys. B* **6**, 2471 (1992).
- M. Yu. Kagan, *Phys. Lett. A* **152**, 303 (1991).
- D. V. Efremov, M. S. Mar’enko, M. A. Baranov, and M. Yu. Kagan, *JETP* **90** (5), 861 (2000).
- M. A. Baranov and M. Yu. Kagan, *Z. Phys. B: Condens. Matter* **86**, 237 (1992).
- A. V. Chubukov, *Phys. Rev. B* **48**, 1097 (1993).
- K. Miyake, S. Schmitt-Rink, and C. M. Varma, *Phys. Rev. B* **34**, 6554 (1986).
- M. Yu. Kagan, M. A. Baranov, and D. V. Efremov, *Physica C (Amsterdam)* **218**, 75 (1993).
- M. Yu. Kagan and V. V. Val’kov, *JETP* **113**(1), 156 (2011).
- J. C. Hubbard, *Proc. R. Soc. London, Ser. A* **276**, 238 (1963).
- D. J. Scalapino, E. Loh, Jr., and J. E. Hirsch, *Phys. Rev. B* **34**, 8190 (1986); D. J. Scalapino, E. Loh, Jr., and J. E. Hirsch, *Phys. Rev. B* **35**, 6694 (1987).
- D. Zanchi and H. J. Schulz, *Phys. Rev. B* **54**, 9509 (1996).
- R. Hlubina, *Phys. Rev. B* **59**, 9600 (1999); J. Mráz and R. Hlubina, *Phys. Rev. B* **67**, 174518 (2003).
- F. Guinea, R. S. Markiewicz, and M. A. H. Vozmediano, *Phys. Rev. B* **69**, 054509 (2004).
- S. Raghu, S. A. Kivelson, and D. J. Scalapino, *Phys. Rev. B* **81**, 224505 (2010).
- J. González, *Phys. Rev. B* **78**, 205431 (2008).
- R. Nandkishore, L. S. Levitov, and A. V. Chubukov, *Nature Phys.* **8** (2), 158 (2012). doi:10.1038/nphys2208
- M. S. Marienko, J. D. Sau, and S. Tewari, arXiv:1202.5784v1.
- A. S. Alexandrov and V. V. Kabanov, *Phys. Rev. Lett.* **106**, 136403 (2011).
- M. Yu. Kagan, D. V. Efremov, M. S. Marienko, and V. V. Val’kov, *JETP Lett.* **93** (12), 725 (2011).
- S. Shubin and S. Vonsovsky, *Proc. R. Soc. London, Ser. A* **145**, 159 (1934).
- S. Shubin and S. Vonsovsky, *Phys. Z. Sowjetunion* **7**, 292 (1935); S. Shubin and S. Vonsovsky, *Phys. Z. Sowjetunion* **10**, 348 (1936).
- S. V. Vonsovsky and M. I. Katsnelson, *J. Phys. C: Solid State Phys.* **12**, 2043 (1979); S. V. Vonsovsky and M. I. Katsnelson, *J. Phys. C: Solid State Phys.* **12**, 2055 (1979).
- R. O. Zaitsev, *Sov. Phys. JETP* **51** (3), 571 (1980).
- R. O. Zaitsev, V. A. Ivanov, and Yu. V. Mikhailova, *Fiz. Met. Metalloved.* **65**, 1032 (1988); R. O. Zaitsev, V. A. Ivanov, and Yu. V. Mikhailova, *Fiz. Met. Metalloved.* **65**, 1108 (1989).
- R. O. Zaitsev, *JETP* **98** (4), 780 (2004).
- V. V. Val’kov and M. M. Korovushkin, *JETP* **112** (1), 108 (2011).
- S. Raghu, E. Berg, A. V. Chubukov, and S. A. Kivelson, *Phys. Rev. B* **85**, 024516 (2012).

<sup>†</sup> Deceased.

40. V. M. Galitskii, *Sov. Phys. JETP* **7**, 104 (1958).
41. P. Bloom, *Phys. Rev. B* **12**, 125 (1975).
42. L. P. Gor'kov and T. K. Melik-Barkhudarov, *Sov. Phys. JETP* **13**, 1018 (1961).
43. L. D. Landau and E. M. Lifshitz, *Course of Theoretical Physics*, Volume 3: *Quantum Mechanics: Non-Relativistic Theory* (Nauka, Moscow, 1989; Butterworth–Heinemann, Oxford, 1991).
44. M. Yu. Kagan, V. V. Val'kov, V. A. Mitskan, and M. M. Korovushkin, *JETP Lett.* **97**(4), 226 (2013).
45. I. E. Dzyaloshinskii and V. M. Yakovenko, *Sov. Phys. JETP* **67** (4), 844 (1988); I. E. Dzyaloshinskii, I. M. Krichever, and Ya. Khronok, *Sov. Phys. JETP* **67** (7), 1492 (1988).
46. K. Okazaki, Y. Ota, Y. Kotani, W. Malaeb, Y. Ishida, T. Shimojima, T. Kiss, S. Watanabe, C.-T. Chen, K. Kihou, C. H. Lee, A. Iyo, H. Eisaki, T. Saito, H. Fukazawa, Y. Kohori, K. Hashimoto, T. Shibauchi, Y. Matsuda, H. Ikeda, H. Miyahara, R. Arita, A. Chai-nani, and S. Shin, *Science* **337**, 1314 (2012).
47. D. Rainer and J. W. Serene, *Phys. Rev. B* **13**, 4745 (1976).
48. M. A. Baranov, D. V. Efremov, M. Yu. Kagan, M. S. Mar'enko, and H. W. Capel, *JETP Lett.* **59** (4), 290 (1994).
49. R. Nandkishore and A. V. Chubukov, *Phys. Rev. B* **86**, 115426 (2012).
50. M. Sigrist and K. Ueda, *Rev. Mod. Phys.* **63**, 239 (1991).
51. A. P. Mackenzie and Y. Maeno, *Rev. Mod. Phys.* **75**, 657 (2003).
52. J. C. Hubbard, *Proc. R. Soc. London, Ser. A* **285**, 542 (1965).
53. P. W. Anderson, *Science* **235**, 1196 (1987).
54. M. Yu. Kagan and T. M. Rice, *J. Phys.: Condens. Mat-ter* **6**, 3771 (1994).
55. Yu. A. Izyumov, *Phys.—Usp.* **40** (5), 445 (1997).
56. N. M. Plakida, *JETP Lett.* **74** (1), 36 (2001); N. M. Plakida, L. Anton, S. Adam, and Gh. Adam, *JETP* **97** (2), 331 (2003).
57. N. M. Plakida and V. S. Oudovenko, *Eur. Phys. J. B* **86**, 115 (2013); N. M. Plakida and V. S. Oudovenko, arXiv:1301.4347v1.

*Translated by M. Sapozhnikov*